

UNCERTAINTY QUANTIFICATION OF AERODYNAMIC AND AEROELASTIC RESPONSES OF A SHORT-GAP TWIN-BOX DECK DEPENDING ON THE WIND ANGLE OF ATTACK

GIUSEPPE G. LOBRIGLIO¹, ANTONIO J. ÁLVAREZ², FELIX NIETO²,
SANTIAGO HERNÁNDEZ² & JOSÉ Á. JURADO²

¹ Faculty of Engineering, University of Pavia, Pavia, Italy.

² School of Civil Engineering, University of La Corunna, Spain.

ABSTRACT

Today, the assessment of the safety of long-span bridges relies on wind tunnel testing, although CFD methods are steadily penetrating in research and industrial practice. The evaluation of force coefficients and flutter derivatives presents multiple uncertainties, related with inflow boundary conditions, mechanical and mathematical models or parameter choices. In this work, we focus on one single uncertainty parameter that is the wind angle of incidence, which has been studied for instance in building aerodynamics. The assumed input probability density function adopted for the angle of incidence has been uniform in the range of angles considered. Uncertainty quantification tools, such as the stochastic collocation method, are used to propagate the uncertainty in the wind angle of attack for the force coefficients and flutter derivatives of a twin-box bridge deck. To this end, 5 2D URANS static simulations have been completed to quantify the uncertainty in the force coefficients, and 70 2D URANS forced oscillation simulations have been required to obtain the stochastic mean and standard deviation of the flutter derivatives, applying nested Clenshaw–Curtis quadrature points at level 3. It has been found that for the force coefficients, the stochastic standard deviation has been up to 0.032 for the lift coefficient. Furthermore, for the aeroelastic response, the flutter derivatives H_1^* , A_1^* , H_2^* and A_2^* show important stochastic standard deviations relative to the stochastic mean value for reduced velocities above 10.

Keywords: aerodynamic derivatives, flutter, force coefficients, stochastic collocation, twin-box deck, uncertainty quantification.

1 INTRODUCTION

The assessment of wind actions is paramount in long-span bridge design. Wind load models require force coefficients and aerodynamic derivatives, among other parameters, to evaluate static deflections due to wind, critical flutter speed or buffeting response.

In bridge engineering practice, the standard procedure for identifying force coefficients and aerodynamic derivatives is to conduct wind tunnel tests of scaled sectional models of the bridge deck. However, experimental measurements are prone to uncertainties in a number of parameters: for instance, experimental measurement errors, insufficient characterization of turbulent flow properties, inaccuracies in the geometry of the sectional model [1] or dispersion in the dynamic properties of the sectional model such as frequencies and/or damping ratios [2]. Several authors have remarked the importance of uncertainties associated with inflow boundary conditions such as angle of attack (AoA), turbulence intensity or length scale [3–6]. In this study, the focus has been put on the sensitivity of force coefficients and aerodynamic derivatives to the uncertainty in the wind angle of attack, which has not been systematically studied in bridge engineering applications to date.

The deterministic realizations of the quantities of interest that are used for the stochastic collocation (SC) have been obtained by means of 2D URANS simulations. In this work, the effect introduced by specific model choices such as the turbulence modelling approach or numerical schemes has not been addressed. The aim of this piece of research is to gain some understanding about the impact that uncertainty in the inflow angle of attack causes in quantities of interest in bridge engineering practice such as force coefficients and aerodynamic derivatives that play a key role in the structure's flutter and buffeting performance.

The remainder of this article is organized as follows: first, the fundamental formulation for wind actions is summarized, while the stochastic collocation method is formally introduced and formulated. Afterwards, the computational approach adopted for numerically obtaining the deterministic realizations of the quantities of interest is described. Then, the application case, which is a short-gap twin-box bridge deck previously studied by the authors, is introduced, and the results of the uncertainty propagation study are reported. Stochastic mean and standard deviations of the force coefficients and aerodynamic derivatives are reported for levels 2 and 3 quadrature points, discussing the convergence of the method and its dependency with individual aerodynamic derivatives and reduced velocities. The paper ends summarizing the main conclusions of the study.

2 FORMULATION

2.1 Aerodynamic and aeroelastic loads

The mean action of wind on a bridge deck may be evaluated by means of the force coefficients that are the non-dimensional expressions of the time-averaged forces and moment on the deck per unit of span length. The corresponding expressions are:

$$C_D = \frac{D}{\frac{1}{2}\rho U^2 B}, C_L = \frac{L}{\frac{1}{2}\rho U^2 B}, C_M = \frac{M}{\frac{1}{2}\rho U^2 B^2}, \quad (1)$$

where D is the mean drag force, positive in the along-wind direction; L is the mean lift force, positive upwards; and M is the mean twist moment, positive in the clockwise direction; all of them expressed per unit of span length. Besides, ρ is the air density, U is the reference wind speed and B is the total width of the deck.

Flutter is a self-excited phenomenon where aerodynamic forces acting on the bridge couple with its motion [7, 8]. Considering two degrees of freedom, heave h and pitch α , the self-excited forces L_{ae} and M_{ae} per unit of span length may be written adopting the semi-empirical approach proposed in [9]:

$$L_{ae} = \frac{1}{2}\rho U^2 B \left[KH_1^* \frac{\dot{h}}{U} + KH_2^* \frac{\dot{\alpha}}{U} + K^2 H_3^* \alpha + K^2 H_4^* \frac{h}{B} \right], \quad (2)$$

$$M_{ae} = \frac{1}{2}\rho U^2 B \left[KA_1^* \frac{\dot{h}}{U} + KA_2^* \frac{\dot{\alpha}}{U} + K^2 A_3^* \alpha + K^2 A_4^* \frac{h}{B} \right], \quad (3)$$

where $K = (B\omega) / U$ is the reduced frequency, being ω the circular frequency of oscillation, the $\dot{}$ symbol represents the time-derivative operation and H_i^* and A_i^* ($i = 1, \dots, 4$) are the aerodynamic derivatives, which are empirical parameters identified by means of wind tunnel tests or numerical simulations. Positive self-excited loads and displacements are considered in the upward and the counterclockwise directions.

2.2 Interpolation curves and stochastic mean and variance

The interpolation points are the Clenshaw–Curtis points in the range $[-1,1]$, which can be transformed afterwards to match the variable of interest range $[a,b]$. For the different levels of quadrature approximation, the number of points (M_l) is for level 1 $M_l = 1$; meanwhile, for any other level, it is $M_l = 2^l + 1$. The coordinates for the points are given by eqn. (4):

$$q_l^m = -\cos \frac{\pi(m-1)}{M_l-1}, m = 1, \dots, M_l. \quad (4)$$

Therefore, the set of points for a given level is,

$$\Theta_l^{(1)} = \{q_l^1, \dots, q_l^{M_l}\} \quad (5)$$

where (1) stands for one dimensional. In case of having a number p of dependent variables, the sparse grid of points is calculated as:

$$\Theta_l^{(p)} = \bigcup_{|l'| \leq l+p-1} \Theta_{l'}^{(1)} \times \dots \times \Theta_{l_p}^{(1)}, |l'| = \sum_{i=1}^p l_i. \quad (6)$$

Thus, for $p = 2$ and $l = 3$, the coordinates will be:

$$\begin{aligned} \Theta_3^{(2)} = & \left(\Theta_1^{(1)} \times \Theta_1^{(1)} \right) \cup \left(\Theta_1^{(1)} \times \Theta_2^{(1)} \right) \cup \left(\Theta_1^{(1)} \times \Theta_3^{(1)} \right) \cup \left(\Theta_2^{(1)} \times \Theta_1^{(1)} \right) \\ & \cup \left(\Theta_2^{(1)} \times \Theta_2^{(1)} \right) \cup \left(\Theta_3^{(1)} \times \Theta_1^{(1)} \right). \end{aligned} \quad (7)$$

The interpolation polynomials are the Lagrange polynomials, whose formulation is presented in eqns (8) and (9),

$$u^{M_l}(q) = \sum_{m=1}^{M_l} u^m L_m(q), \quad (8)$$

$$L_m(q) = \prod_{\substack{j=0 \\ j \neq m}}^{M_l} \frac{q - q^j}{q^m - q^j} = \frac{(q - q^1) \cdots (q - q^{m-1})(q - q^{m+1}) \cdots (q - q^{M_l})}{(q^m - q^1) \cdots (q^m - q^{m-1})(q^m - q^{m+1}) \cdots (q^m - q^{M_l})}, \quad (9)$$

where u^m are the values of the parameters of interest at the interpolation points. By construction, the Lagrange polynomials satisfy:

$$L_m(q^n) = \delta_{nm}, 1 \leq m, n \leq M_l \Rightarrow u^{M_l}(q^m) = u^m. \quad (10)$$

Then, the multidimensional interpolation surface is

$$\mathcal{J}_l^{(p)} \mathbf{u} = \sum_{|l| \leq l+p-1} \left(\Delta_{l_1}^{(1)} \otimes \cdots \otimes \Delta_{l_p}^{(1)} \right), \quad (11)$$

where \otimes stands for tensor product, and

$$\Delta_l^{(1)} \mathbf{u} = \left(\mathcal{J}_l^{(1)} - \mathcal{J}_{l-1}^{(1)} \right) \mathbf{u}, \mathcal{J}_0^{(1)} \mathbf{u} = 0, \mathcal{J}_l^{(1)} \mathbf{u} = \sum_{m=1}^{M_l} \mathbf{u}^m L_m(q). \quad (12)$$

The calculation of the stochastic mean and variance for the one-dimensional case is defined in eqns (13) and (14):

$$\mu_l^{(1)}(u) = \int u f(q) dq \approx \sum_{m=1}^{M_l} u^m w_m, w_m = \int_{-1}^1 L_m(q) f(q) dq, \quad (13)$$

$$\sigma_l^{2(1)} \approx \sum_{m=1}^{M_l} (u^m)^2 w_m - \left(\sum_{m=1}^{M_l} u^m w_m \right)^2. \quad (14)$$

Finally, the mean and variance for the multidimensional case are calculated as shown in eqns (15) – (18):

$$\mu_l^{(p)}(\mathbf{u}) = \sum_{|l| \leq l+p-1} \left(\Delta \mathcal{M}_{l_1}^{(1)} \otimes \cdots \otimes \Delta \mathcal{M}_{l_p}^{(1)} \right) \mathbf{u}, \quad (15)$$

$$\Delta \mathcal{M}_{l_i}^{(1)} \mathbf{u} = \left(\mathcal{M}_{l_i}^{(1)} - \mathcal{M}_{l_i-1}^{(1)} \right) \mathbf{u}, \mathcal{M}_0^{(1)} \mathbf{u} = 0, \mathcal{M}_{l_i}^{(1)} \mathbf{u} = \mu_{l_i}^{(1)}(\mathbf{u}), \quad (16)$$

$$\sigma_l^{2(p)}(\mathbf{u}) = \sum_{|l| \leq l+p-1} \left(\Delta \mathcal{V}_{l_1}^{(1)} \otimes \cdots \otimes \Delta \mathcal{V}_{l_p}^{(1)} \right) \mathbf{u}, \quad (17)$$

$$\Delta \mathcal{V}_{l_i}^{(1)} \mathbf{u} = \left(\mathcal{V}_{l_i}^{(1)} - \mathcal{V}_{l_i-1}^{(1)} \right) \mathbf{u}, \mathcal{V}_0^{(1)} \mathbf{u} = 0, \mathcal{V}_{l_i}^{(1)} \mathbf{u} = \sigma_{l_i}^{2(1)}. \quad (18)$$

Further information can be found in [10, 4].

3 COMPUTATIONAL APPROACH

The deterministic samples of the quantities of interest, that are latter used in the stochastic collocation, are identified by means of CFD simulations. To this end, 2D URANS simulations are conducted for the short-gap twin-box deck named as g22 case in [11], which has been adopted as case of study (see Section 4 for details). The turbulence model of choice has been $k-\omega$ SST. All the simulations have been conducted at $Re_C = 1.14 \cdot 10^5$, adopting a turbulence intensity of 1.55% and a turbulent length scale of $0.1C$, being C the width of a single box. The length of the slot between boxes is $0.224C$ and the depth is $0.134C$.

The layout of the flow domain is the one reported in the authors' previous work [11]. Similarly, the mesh adopted in this study is the medium grid in the spatial verification study

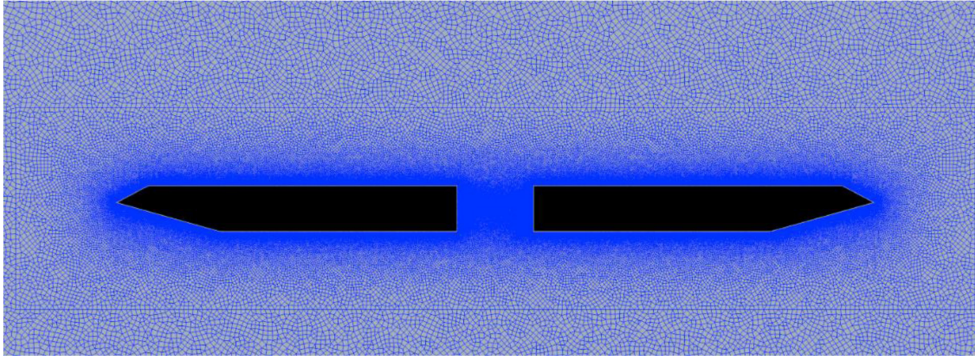


Figure 1: Detail of the geometry and mesh for the g22 twin-box cross-section.

reported in the same reference for the g22 case, using the same type of boundary conditions. In this piece of research, the maximum Courant number imposed has been 1. In Fig. 1, an image of the studied twin-box deck geometry and the mesh surrounding it is provided.

In the numerical simulations, the interpolation from cell centres to face centres has been carried out adopting a central differencing scheme, while gradient terms have been discretized using a second-order cell limited scheme. For the Laplacian terms, the Gauss discretization is combined with linear and limited interpolations for the surface normal scheme. For the divergence terms, Gaussian discretization has been used combined with linear, linear upwind and upwind interpolation schemes depending on the considered variables. For the surface normal gradient terms, a limited non-orthogonal correction scheme has been adopted. For the time schemes, the Euler scheme has been selected based on the imposed maximum Courant number of one.

It has been checked that integral parameters obtained for the case of study are very similar to the numerical ones in [11] despite the minor differences in the value of the turbulence intensity and numerical settings. Furthermore, the results obtained herein are aligned with the experimental results reported in the same reference.

The evaluation of the flutter derivatives is based on one degree of freedom forced oscillation simulations in heave and pitch. The reference flow velocity at the inlet is the same in all the simulations, modifying the frequency of oscillation in order to cover the desired range of reduced velocities (0, 20). The amplitudes of oscillation adopted in this work have been 3° and 0.02 m.

4 APPLICATION CASE

4.1 Description

In this application case, a single uncertainty parameter, the wind angle of attack, is considered. This parameter aims at representing the uncertainty in the inflow boundary conditions in wind tunnel experiments. To this end, a uniform distribution between -1° and $+1^\circ$ in the random variable is considered. This uncertainty is propagated to the quantities of interest that are the integral parameters and the aerodynamic derivatives for the short-gap twin-box deck named as g22, previously introduced. Other uncertainties present in experiments or numerical simulations are not considered.

In the following, the stochastic collocation (SC) method is applied for a single random variable. Once a number of deterministic samples are obtained by means of CFD simula-

Table 1: Level 3 Clenshaw–Curtis deterministic samples for the integral parameters of the g22 cross-section.

AoA(°)	C_D	C_L	C_M	Std(C_D)	Std(C_L)	Std(C_M)
1.00	0.038	-0.084	0.035	0.0053	0.1572	0.0106
0.707	0.039	-0.104	0.029	0.0055	0.1581	0.0109
0.00	0.039	-0.152	0.014	0.0060	0.1588	0.0113
-0.707	0.024	-0.179	-0.0008	0.0000	0.0008	0.0002
-1.00	0.023	-0.201	-0.007	0.0000	0.0005	0.0002

tions at quadrature points, Lagrange polynomials are interpolated. Clenshaw–Curtis points are adopted as nested quadrature points, following the method in [4]. Aiming at keeping a reasonable computational burden, level 2 and level 3 Clenshaw–Curtis points have been considered, which has demanded 5 2D URANS simulation for uncertainty propagation of the integral parameters, and 70 forced oscillation 2D URANS simulation to ascertain the uncertainty propagation in the flutter derivatives. The convergence of the method is assessed comparing stochastic results and cumulative distribution functions (CDFs) for the same outputs at different Clenshaw–Curtis levels.

4.2 Stochastic values for the integral parameters

The numerical results for the deterministic samples of the level 3 quadrature points for the force coefficients for the g22 twin-box cross-section are reported in Table 1. Positive slopes for the lift and moment coefficients depending on the angle of attack are identified, which is in agreement with the expected aeroelastic behaviour of this type of efficient deck cross-section.

Similarly, stochastic mean and standard deviation values of the integral parameters for level 2 and level 3 are reported in Table 2. The examination of the values in this table signals a reasonable convergence for the level 3 stochastic values when compared with the stochastic statistics belonging to level 2. Only the standard deviation of the lift coefficient shows appreciable differences for both the stochastic mean and standard deviations, which

Table 2: Stochastic mean and standard deviation of the integral parameters of the g22 cross-section at levels 1, 2 and 3.

Stochastic statistics	Level	C_D	C_L	C_M	Std(C_D)	Std(C_L)	Std(C_M)
mean	1	0.039	-0.152	0.014	0.006	0.159	0.011
	2	0.036	-0.149	0.014	0.005	0.132	0.009
	3	0.034	-0.146	0.014	0.004	0.111	0.008
standard deviation	1	0.000	0.000	0.000	0.000	0.000	0.000
	2	0.006	0.034	0.012	0.002	0.059	0.004
	3	0.007	0.032	0.012	0.003	0.072	0.005

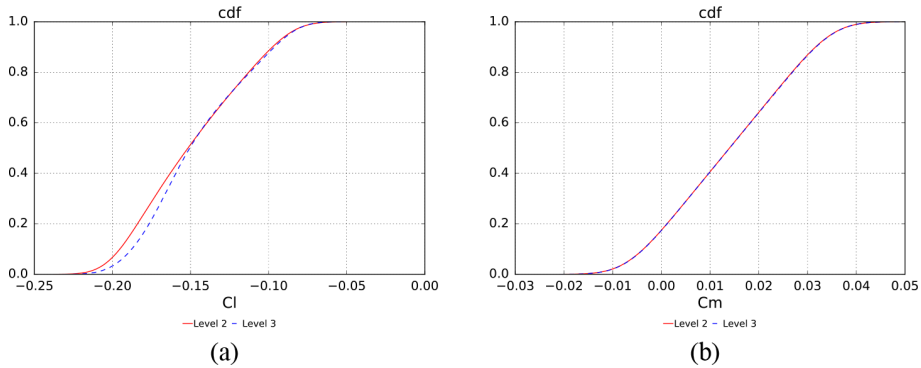


Figure 2: Comparison between level 2 and level 3 stochastic collocation for the cumulative distribution functions. (a) Lift coefficient; (b) moment coefficient.

are related with the almost null values identified at negative angles of attack and the difficulty to accurately approximate the behaviour of this quantity with a small number of quadrature points. In order to better ascertain the level of convergence attained with level 2 and level 3 quadrature points, the cumulative distribution functions for a selection of integral parameters are reported in Fig.2.

The importance of the uncertainty in the wind angle of attack in the force coefficients may be further assessed by comparing the stochastic mean \pm stochastic standard deviation obtained using 2D URANS simulations with the wind tunnel values in [11]. The results are reported in Fig. 3 for levels 2 and 3 quadrature points, and it should be noticed how the wind tunnel values are within the interval defined by the stochastic mean and standard deviation of the drag and lift coefficients, while for the moment coefficient, the experimental value is remarkably close to the aforementioned interval.

4.3 Stochastic values for the aerodynamic derivatives

In Fig. 4, the experimental values of the aerodynamic derivatives obtained for the g22 cross-section[11] obtained by free-vibration tests are reported along with the stochastic mean \pm the stochastic standard deviation for levels 2 and 3 quadrature points for the H_i^* and A_i^* ($i = 1, \dots, 4$) aerodynamic derivatives obtained computationally by means of forced oscillation simulations. The general agreement between experimental and numerical values is good for aerodynamic derivatives; however, some discrepancies are evident for H_2^* and A_2^* . It should be noticed that the comparison is being made among experimental results obtained by means of free oscillation wind tunnel tests and forced oscillation numerical simulations. These are the two approaches generally adopted to extract aerodynamic derivatives, and they have shown frequently discrepancies among them, even when the two techniques have been applied in wind tunnel experiments. In [12], it is apparent the change in sign obtained at high reduced velocities for the H_2^* aerodynamic derivative for the slotted box girder depending on the experimental method adopted to extract flutter derivatives. Furthermore, the aerodynamic derivatives related with the deck's velocity of rotation, H_2^* and A_2^* , have traditionally posed a challenge for 2D URANS simulations [13–16].

Focusing on the propagation of the uncertainty in the flow angle of attack, Fig. 4 shows that the sensitivity of the aerodynamic derivatives is in general low with respect to this input.

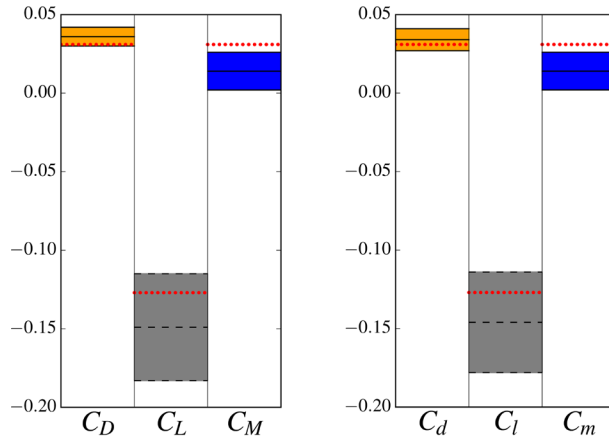


Figure 3: Stochastic mean \pm stochastic standard deviation for the force coefficients including experimental values as dotted red lines. (a) Level 2 quadrature points; (b) level 3 quadrature points.

In fact, the stochastic standard deviation of the aerodynamic derivatives is important only for relatively high reduced velocities. It should be noted that there are many more sources of uncertainty in the experimental extraction of the aerodynamic derivatives such as the damping of the sectional model, which cannot be considered by means of forced oscillation simulations. Another issue that requires a careful discussion is the convergence obtained using level 3 quadrature points. In Table 3, the relative differences in the stochastic mean of the aerodynamic derivatives between level 2 and level 3 points are reported. In general, the stochastic means

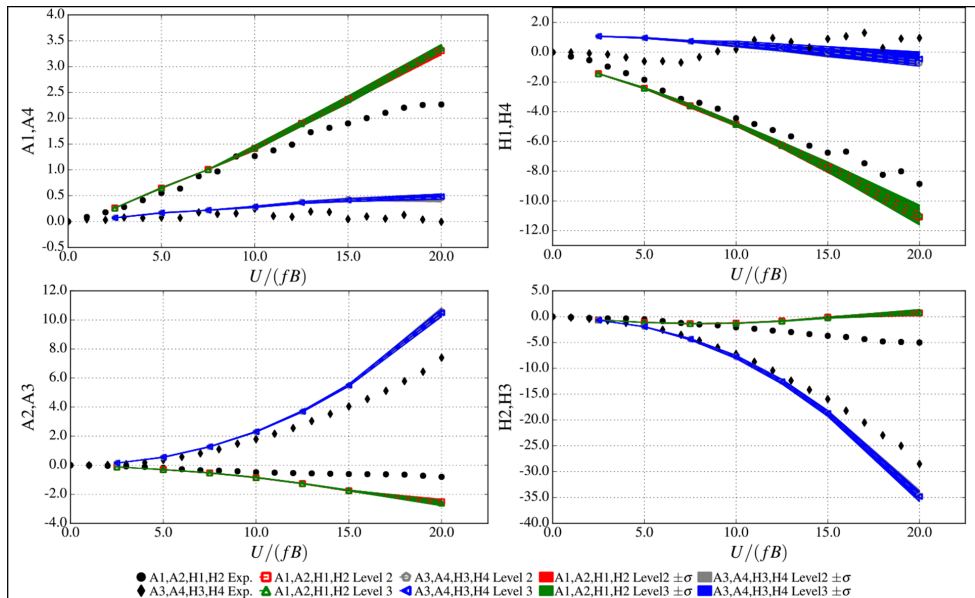


Figure 4: Stochastic mean \pm stochastic standard deviation for the aerodynamic derivatives including experimental values taken from [11].

Table 3: Relative difference (%) in the stochastic mean of the aerodynamic derivatives between level 2 and level 3 quadrature points. Relative differences between 1% and 5% are marked in yellow, between 5% and 10% are marked in orange, and differences above 10% are marked in red.

U_R	H_1^*	H_2^*	H_3^*	A_1^*	A_2^*	A_3^*
2.5	0.07	0.15	0.13	0.40	0.21	0.02
5	0.15	0.29	0.03	0.00	0.76	0.70
7.5	0.67	0.47	0.25	0.10	0.84	0.44
10	0.11	1.88	0.43	0.95	1.15	0.48
12.5	0.57	6.53	0.32	0.27	0.65	0.58
15	0.71	86.02	0.10	0.32	1.28	0.36
20	1.15	22.35	0.36	1.46	3.96	1.03

of the aerodynamic derivatives have reached convergence, although relative differences above 1% are identified at $U_R = 20$, and the H_2^* aerodynamic derivative presents relative differences higher than 10% for $U_R \geq 15$, precisely at the change in sign in the aerodynamic derivative, that is not present in the experimental tests used for validation. Furthermore, these results show that the level of the quadrature adopted in the stochastic collocation depends on the reduced velocity to be reached and the particular aerodynamic derivative to be studied. In this application case, this means that if an increase in the quadrature points is required for a more accurate evaluation of the stochastic mean of the H_2^* and A_2^* derivatives, only additional CFD simulations related with the pitch degree of freedom would be required, saving in this manner valuable computer resources.

The analysis of the convergence in the stochastic standard deviation requires also a comparison between level 2 and level 3 results relative to the stochastic mean value of each aerodynamic derivative in order to relate the scattering in the aerodynamic derivative with the value of the derivative itself at the corresponding reduced velocity. In Table 4, the relative

Table 4: Difference in the stochastic standard deviation between levels 2 and 3 quadrature points relative to the level 3 stochastic mean of the flutter derivatives in %. Relative differences between 1% and 5% are marked in yellow, and differences above 10% are marked in red.

U_R	H_1^*	H_2^*	H_3^*	A_1^*	A_2^*	A_3^*
2.5	0.14	0.06	0.02	0.54	0.23	0.13
5	0.08	0.32	0.45	0.15	0.01	1.19
7.5	0.92	0.52	0.06	0.20	0.28	0.67
10	0.39	2.03	0.05	0.33	0.18	0.66
12.5	0.09	4.57	0.01	0.38	0.17	0.62
15	0.15	23.72	0.07	0.41	0.41	0.80
20	3.44	3.31	0.44	0.20	0.34	0.22

differences are reported, showing again that is the H_2^* aerodynamic derivative the only one presenting a limited convergence at high reduced velocities.

5 CONCLUSIONS

In this work, the results obtained in the wind angle of attack uncertainty propagation study conducted for quantities of interest such as force coefficients and aerodynamic derivatives of a twin-box bridge deck are reported. Moreover, the general procedure based on the application of the stochastic collocation method and the use of CFD simulations to obtain the deterministic samples has been described. It has been found that the level 3 approximation has provided converged stochastic statistics for the force coefficients. For the aerodynamic derivatives, the sensitivity of these quantities to uncertainties in the angle of attack has been found to be quite limited within the considered range for the random variable. Interestingly, the stochastic convergence has been found to be dependent on the reduced velocity magnitude and the particular aerodynamic derivative under consideration.

This study may be further developed by including additional sources of uncertainty such as inflow turbulent intensity or the precise geometric definition of the model under study.

ACKNOWLEDGEMENTS

This research has been funded by the Spanish Ministry for Science and Innovation, in the frame of the research project PID2019-110786GB-I00, and the Xunta de Galicia (Galician Regional Government), including FEDER funding, with program reference ED431C 2017/72. Giuseppe G. Lobriglio has been funded by an Erasmus+ Higher Education Traineeship. The authors fully acknowledge the support received.

REFERENCES

- [1] Mannini, C., Soda, A., Voß, R. & Schewe, G., Unsteady RANS simulations of flow around a bridge section. *Journal of Wind Engineering and Industrial Aerodynamics*, **98**, pp. 724–753, 2010. <https://doi.org/10.1016/j.jweia.2010.06.010>
- [2] Fang, G., Cao, J., Yang, Y., Zhao, L., Cao, S. & Ge, Y., Experimental uncertainty quantification of flutter derivatives for a PK section girder and its application on probabilistic flutter analysis. *ASCE Journal of Bridge Engineering*, **25(7)**, Article number: 04020034, 2020. [https://doi.org/10.1061/\(asce\)be.1943-5592.0001567](https://doi.org/10.1061/(asce)be.1943-5592.0001567)
- [3] Bruno, L. & Fransos, D., Probabilistic evaluation of the aerodynamic properties of a bridge deck. *Journal of Wind Engineering and Industrial Aerodynamics*, **99**, pp. 718–728, 2011. <https://doi.org/10.1016/j.jweia.2011.03.007>
- [4] Mariotti, A., Salvetti, M.V., Omrani, P.S. & Witteveen, J.A.S., Stochastic analysis of the impact of freestream conditions on the aerodynamics of a rectangular 5:1 cylinder. *Computers and Fluids*, **136**, pp. 170–192, 2016. <https://doi.org/10.1016/j.compfluid.2016.06.008>
- [5] Lamberti, G. & Gorlé, C., Uncertainty quantification for RANS predictions of wind loads on buildings. In *Proc. INVENTO 2018, LNCE 24*, Ricciardelli, F. & Avossa, A.M. eds., pp. 402–412, 2019.
- [6] Lamberti, G. & Gorlé, C., Sensitivity of LES predictions of wind loading on a high-rise building to the inflow boundary condition. *Journal of Wind Engineering and Industrial Aerodynamics*, **206**, Article number: 104370, 2020. <https://doi.org/10.1016/j.jweia.2020.104370>

- [7] Xu, Y.L., *Wind Effects on Cable-Supported Bridges*. John Wiley & Sons; Singapore Pte. Ltd, 2013.
- [8] Jurado, J.Á., Hernández, S., Nieto, F. & Mosquera, A., *Bridge aeroelasticity. Sensitivity analysis and optimal design*. WITPress, Southampton, UK, 2011.
- [9] Scanlan, R.H. & Tomko, J.J., Airfoil and bridge deck flutter derivatives. *Journal of the Engineering Mechanics Division*, **97(6)**, pp. 1717–1737, 1971. <https://doi.org/10.1061/jmcea3.0001526>
- [10] Smith, R.C., *Uncertainty quantification. Theory, implementation, and applications*, SIAM, 2014.
- [11] Nieto, F., Cid Montoya, M., Hernández, S., Kusano, I., Casteleiro, A., Álvarez, A.J., Jurado, J.Á. & Fontán, A., Aerodynamic and aeroelastic responses of short gap twin-box decks: Box geometry and gap distance dependent surrogate based design. *Journal of Wind Engineering and Industrial Aerodynamics*, **201**, Article 104147, 2020. <https://doi.org/10.1016/j.jweia.2020.104147>
- [12] Sarkar, P.P., Caracoglia, L., Haan, F. Jr., Sato, H. & Murakoshi, J., Comparative and sensitivity study of flutter derivatives of selected bridge deck sections, Part 1: Analysis of inter-laboratory experimental data. *Engineering Structures*, **31**, pp. 158–169, 2009. <https://doi.org/10.1016/j.engstruct.2008.07.020>
- [13] Sarkic, A., Höffer, R. & Brcic, S., Numerical simulations and experimental validations of force coefficients and flutter derivatives of a bridge deck. *Journal of Wind Engineering and Industrial Aerodynamics*, **144**, pp. 172–182, 2015. <https://doi.org/10.1016/j.jweia.2015.04.017>
- [14] Nieto, F., Owen, J.S., Hargreaves, D.M. & Hernández, S., Bridge deck flutter derivatives: Efficient numerical evaluation exploiting their interdependence. *Journal of Wind Engineering and Industrial Aerodynamics*, **136**, pp. 138–150, 2015. <https://doi.org/10.1016/j.jweia.2014.11.006>
- [15] Patruno, L., Accuracy of numerically evaluated flutter derivatives of bridge deck sections using RANS: Effects on the flutter onset velocity. *Engineering Structures*, **89**, pp. 49–65, 2015. <https://doi.org/10.1016/j.engstruct.2015.01.034>
- [16] Sarkic, A., Fisch, R., Höffer, R. & Bletzinger, K.U., Bridge flutter derivatives based on computed, validated pressure fields. *Journal of Wind Engineering and Industrial Aerodynamics*, **104–106**, pp. 141–151, 2012. <https://doi.org/10.1016/j.jweia.2012.02.033>